Thermochimica Acta, 228 (1993) 345–357
Elsevier Science Publishers B.V., Amsterdam

Masking effect of the ICT features and thermodynamics of *trans*-4-(dimethylamino)-β-(1-naphthyl) styrene

Ibrahim A. Al-Ansari and Moein B. Sayed *
Chemistry Department, Qatar University, Doha-2713 (Qatar)

(Received 10 February 1993; accepted 18 March 1993)

Abstract

Trans-4-(dimethylamino)-β-(1-naphthyl) styrene (DMANS) exhibits a fair ability to undergo intramolecular charge transfer (ICT), which polarizes the molecule into rigid D^+-A^- moieties. This causes the excited molecule to emit anomalous fluorescence; its quantum yield is a function of the rigidity, while its energy is dependent on the polarity. Glycerol affords the most suitable conditions assisting the molecular rigidity and polarity. Low-temperature measurements of DMANS fluorescence in glycerol reveal a drop in the emission half band width and a rise in its energy and intensity on lowering the temperature, with these dependencies being equilibrated near 273 K. This might demonstrate a state of thermodynamic equilibrium. Under ordinary conditions, ICT-induced fluorescence dominates, while emission from the locally excited state becomes increasingly dominant at lower temperatures, probably due to freezing dipole interactions. Protonation-induced masking effect of the lone pair electrons at the amino group quenches both the ICT absorption and fluorescence so that the polarized, rigid molecular structure of DMANS reverts to a more delocalized one. This could be the origin of the solid state phase transition induced in the protonated form. These proton-induced structural shifts are traced by IR and UV spectroscopy, both in absorption and emission as well as thermally by DTA.

INTRODUCTION

Charge transfer (CT) complexes have received great attention since the pioneer work of Berthelot [1]. Among long range compounds possessing the ability to form photo-induced charge transfer complexes are those of intramolecular donor–acceptor (D–A) moieties [2–9], which are termed ICT complexes. Such compounds have found potential applications in lasing dyes, liquid crystals and non-linear optical devices.

Trans-4-(dimethylamino)-β-(1-naphthyl) styrene (DMANS) has been of special interest because of its anomalous emission [10], which is explained in terms of sudden solid state polarization of the D–A—CH=CH– bridge

* Corresponding author.

[11, 12]. The quantum yield of this emission, however is small, and it has been found to be a function of the molecular rigidity to free rotation and/or twisting, since a radiationless energy dissipation [13, 14] could take place via such mechanisms. The fluorescence quantum yield has also been observed to increase in more viscous solvents, e.g. glycerol, which agrees with the free volume dependence of intramolecular rotation in such solvents [15–17].

In the present work, it is anticipated that DMANS would have solid state and solid–liquid phase transitions, which are sensitive to variation in molecular and environmental rigidity. This stimulated the aim of the present structure-guided discussion of the spectral and thermal shifts, which are observed upon masking the role of the lone pair electrons at the $-N(CH_3)_2$ group of DMANS. Such lone pair electrons play the principal role in stabilizing the ICT absorption and fluorescence phenomena. It also affects the molecular mesomerism and hence both the solid state and solid–liquid phase transitions.

EXPERIMENTAL

Procedure

DMANS was prepared following a stepwise Wittig coupling:

The synthesis of 1-chloromethyl naphthalene. In step 1, 0.04 mole of 1-naphthylmethanol (Aldrich) and 0.04 mole thionylchloride (Alfa) were stirred in dry benzene at 300 K, prior to reflux for 5–6 h. The product was extracted from benzene/water as a brown liquid (b.p. 443–448 K).

The synthesis of 1-naphthyl (methyltriphenylphosphoniumchloride). In step 2, 0.04 mole of each of the product of step 1 and triphenylphosphine (Aldrich) were refluxed in dry toluene for 17 h. The chloride product was recrystallized from water (m.p. >573 K).

Synthesis of DMANS (**I**). 0.013 mole of the product of step 2 was flushed with dry nitrogen. 70 cm^3 of dry toluene was injected through a septum cap, followed by 11 cm^3 of 1.18 M ether in cyclohexane, and the mixture was then stirred at 353 K for 1 h. 0.006 mole of dimethylaminobenzaldehyde (dissolved in 50 cm^3 dry xylene) was added dropwise to the reaction mixture, which was refluxed for 24 h. Water was added to dissolve unreacted chlorides. The organic phase was separated and dried over anhydrous Na_2SO_4. DMANS was eventually obtained in high yield and was recrystallized from ethanol as bright yellow crystals (m.p. 378 K).

DMANS was characterized [18] by elemental analysis, mass spectrometry, ^1H- and ^{13}C-NMR, IR and UV spectroscopy. The mass spectrum showed four peaks: the top mass peak M^+ 273.10 (calc. 273.37), $M^+ + 1$ 23.4 (calc. 23.36), $M^+ + 2$ 2.7 (calc. 2.62) and the peak $M^+ - 44$, 24.2% corresponding to the loss of $-N(CH_3)_2$ of 229 m/z.

The preparation of the hydrochloride salt. Pure DMANS was dissolved in dry benzene and exposed to a stream of dry HCl gas. The HCL-salt precipitated as pale yellow crystals (m.p. 438 K).

Methods and equipment

Mass spectra were measured using a Hewlett–Packard 5985 A GC/MS spectrometer operating at 70 eV ionization voltage and 473 K. NMR spectra were measured in $CDCl_3$ at 360 MHz, using a Bruker spectrometer. IR spectra were measured in the solid state, using KBr disks on a Nicolet FT-IR 510P spectrometer. UV spectra were measured on 10^{-7} M solutions of DMANS in pure cyclohexane, acetonitrile, and ethanol and in ethanol only on the HCl salt using a Beckman DU-70 spectrophotometer.

Emission spectra were measured on 10^{-5} M solution in degassed cyclohexane, *n*-hexane, chloroform, diethylether, tetrahydrofuran, acetonitrile, *N,N*-dimethylformamide, dimethylsulphoxide, methanol, ethanol, butanol and glycerol. The measurements were performed in vacuo at 295 K, except for the glycerol solution for which the measurements were carried out at lower temperatures in addition, using the experimental setup [18] previously described. An American Instrument Company (AMINCO) spectrofluorimeter was used, with an excitation source of a Xe–Hg arc lamp operating at 150 W and a Hamamatsu K 446 photomultiplier detector. The emission quantum yield was measured with reference to quinine sulphate in 0.1 N H_2SO_4.

Differential thermal analysis (DTA) was performed in air with 20 mg samples of DMANS and 10 mg of the protonated form, using a Shimadzu DSC TA 30 thermal analyser in the temperature range 273–973 K. The rate of heating was 10 K min^{-1}. The thermal data were treated as prescribed elsewhere [19].

RESULTS AND DISCUSSION

Before initiating a comprehensive discussion on protonation-induced thermal changes and shifts in DMANS, a preliminary structural analysis could be potentially important.

DMANS (**I**) assumes a rigid ICT-polarized structure capable of activating a solid state fluorescence emission [7, 8]; its intensity is a function of both the structural and environmental rigidity [20, 21] and its energy is dependent on the polarity of the medium. Molecular motions, and therefore, solid state phase transitions are hardly possible in such a rigid system. Nevertheless, the ^1H NMR spectral coupling constant at 16 Hz suggests that this compound is present in a trans configuration [22, 23].

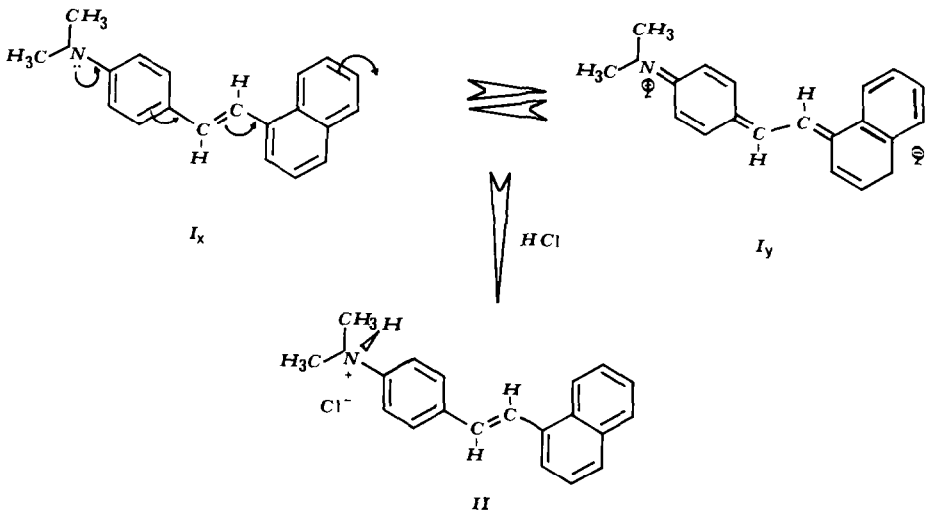

Scheme 1. Proposed structural equilibrium in DMANS shifted towards ICT-stabilized structure $\mathbf{I}_y$ and protonation-induced structural shift into the form **II**.

This, along with the ICT-induced polarization about the D–A bridge, favours the quinonoid structure $\mathbf{I}_y$ over the more delocalized $\mathbf{I}_x$ form (Scheme 1); $\mathbf{I}_y$ formation also assisted in the more polar and viscous media.

A correlative spectral analysis of the role of protonation in converting the rigid quinonoid into the more delocalized structures would provide more supporting evidence in favour of the mechanisms described here.

Spectral analyses

Infrared spectra

The most important spectral feature indicative of the equilibrium shifting towards structure $\mathbf{I}_y$ (Scheme 1) appears at 1725 cm^{-1} (Fig. 1, curve I), with its first overtone at 3430 cm^{-1}. The relatively high frequency of 1725 cm^{-1} favours the assignment to the quinonoid skeleton vibration of the $\mathbf{I}_y$ form more than the weakly IR-active –CH=CH– stretching mode of the more delocalized $\mathbf{I}_x$ form, which should appear at lower frequencies near 1640 cm^{-1}. Protonation at the nitrogen atom results in a more delocalized structure **II** (Scheme 1), which is similar to structure $\mathbf{I}_x$. This consequently results in a spectral shift of the quinonoid skeleton vibration of $\mathbf{I}_y$ at 1725 cm^{-1} to 1644 cm^{-1} (Fig. 1, curve II), which is assigned to the –HC=CH– stretching mode of structure **II**. This indicates that masking the role of the lone pair electrons destabilizes the ICT structure in favour of the more delocalized structure. This implies several consequences on various structural and thermodynamic aspects of DMANS. Evidence of the protonation is clearly explicit in the appearance of new bands at 3468 and

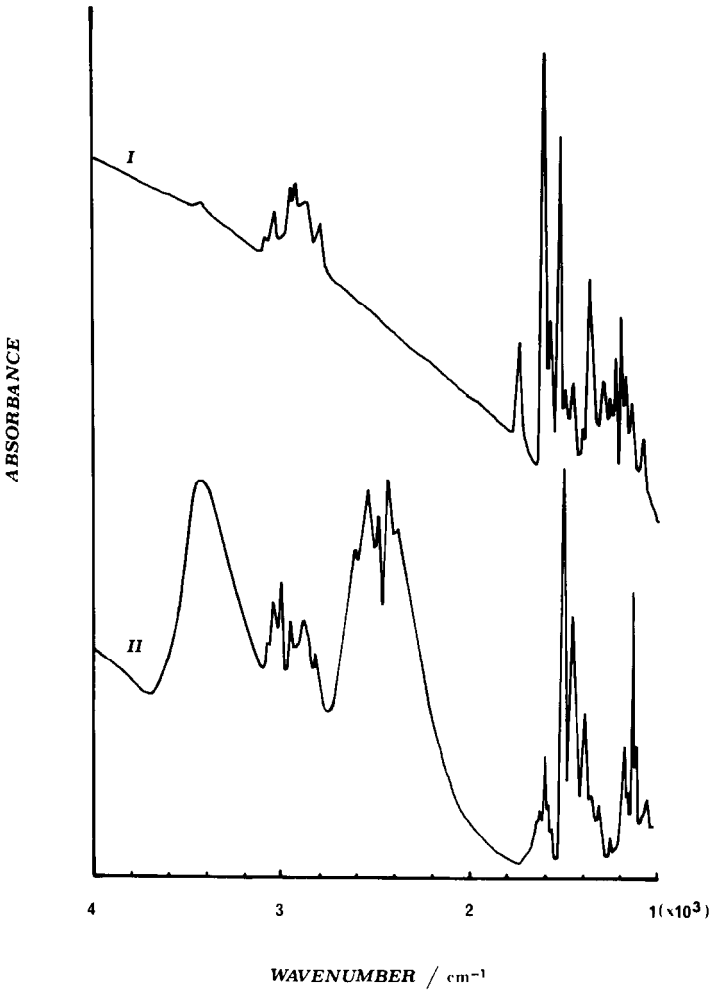

Fig. 1. IR spectra (4000–1000 cm^{-1}) of DMANS (I) and its protonated form (II).

near 2500 cm^{-1} (Fig. 1, curve II) as associated with N^{+}–H stretching vibrations.

Two strong absorptions at 1605 and 1522 cm^{-1} are present in the finger print region, see Fig. 1, curve I. These two bands merge upon protonation into a single band (Fig. 1, curve II) at 1505 cm^{-1}. This is consistent with shifting the molecular structure from the $\mathbf{I}_y$ form with two distinguishable phenyl and naphthyl ring breating modes at 1605 and 1522 cm^{-1} into the more delocalized structure **II** with a typical ring vibration at 1505 cm^{-1}. Consistent with this ICT-induced vibration partition in DMANS, the olefinic =C–H in-plane deformation appears at 1478 and 1442 cm^{-1}, with a spectral shift of $\pm 18\ cm^{-1}$ from its normally observed frequency of 1460 cm^{-1}. The partition in this case is attributed to a location of the

vibrating species in two oppositely charged D^+-A^- moieties. These two absorptions merge upon protonation into a single absorption at 1462 cm^{-1}. Protonation of DMANS may influence the CH_3 vibrations to a lesser extent, which agrees with the positive charge permanently resident on the nitrogen atom in either $\mathbf{I}_y$ or **II**. The asymmetric and symmetric in-plane deformations appear at 1398 and 1362 cm^{-1}, respectively. They only swap intensities on protonation.

It is important to admit that such solid state spectral data of ICT-favoured DMANS may be influenced by the polar matrix of the KBr disc. However, UV-excited emissions from the ICT-state of a self-supported DMANS should reduce the extent to which the KBr matrix stabilizes the ICT complex in the solid state. Assignment of the IR absorption bands was made with respect to previously published data [24].

Ultraviolet absorption spectra

Figure 2 illustrates the effect of varying solvent polarity and viscosity on the UV spectrum of DMANS. The spectrum in cyclohexane (Fig. 2, curve A) shows three bands at 222, 290 and 357 nm. The more dominant

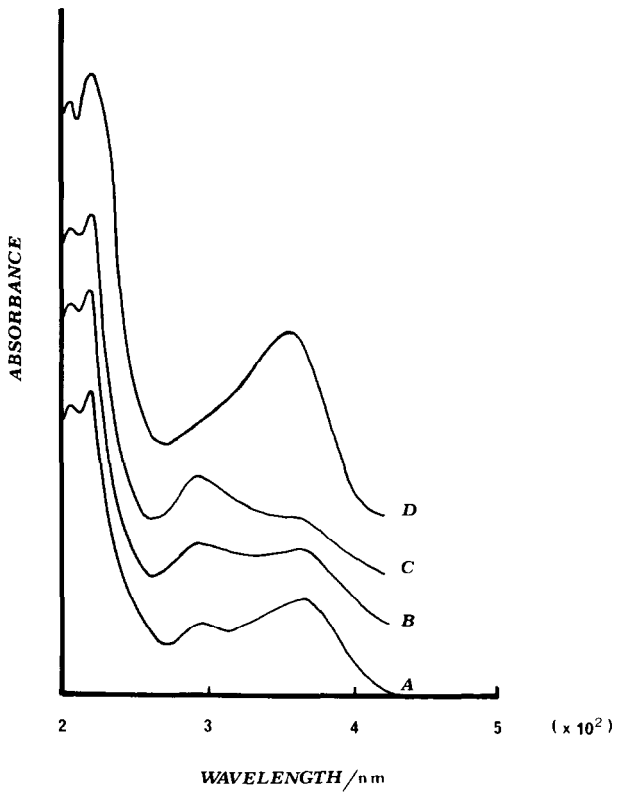

Fig. 2. UV spectra (200–500 nm) of DMANS in cyclohexane (curve A), acetonitrile (curve B), ethenol (curve C) and of its protonated form in ethanol (curve D).

absorption at 222 nm is least sensitive to the solvent parameters; its higher energy suggests that it should be assigned to a $\pi \rightarrow \pi^*$ transition of weakly delocalized π-electrons. At variance, with this, the lower energy of the absorption at 357 nm obviously suggests that it should be assigned to a $\pi \rightarrow \pi^*$ transition of highly delocalized π-electrons. The mid-energy band at 290 nm is, however, similar to the CT band of *N,N*-dimethylaniline [25], and this assigns the latter band to the DMANS ICT transition. The latter absorptions at 290 and 357 nm are most sensitive to solvent polarity and viscosity. The band at 290 nm intensifies (Fig. 2, curve B) at the expense of the band at 357 nm upon replacing cyclohexane with the more polar acetonitrile. Ethanol, however is less polar than acetonitrile, exaggerates the solvent effect, see Fig. 2, curve C, and could be attributed to its higher viscosity. The hyperchromic shift at 290 nm, together with the hypochromic shift at 357 nm, would explain an equilibrium shifted to the $\mathbf{I}_y$ form in the more polar and more viscous solvents and to the $\mathbf{I}_x$ form in the less polar and less viscous solvents. Nevertheless, the ICT band at 290 nm is clearly evident in all cases, which is consistent with the solid state IR spectroscopic data indicating self ICT-stabilized structure $\mathbf{I}_y$.

The UV spectrum of the protonated form (Fig. 2, curve D) reveals supporting evidence for destruction of the ICT structure. This is shown by two aspects: disappearance of the ICT band at 290 nm and the hyperchromic shift at 357 nm of the band assigned to the $\pi \rightarrow \pi^*$ transition of the highly delocalized structure **II**, which is similar to structure $\mathbf{I}_x$ of DMANS. These protonation-induced spectral shifts would also confirm the preceding UV band assignment of DMANS.

UV-excited fluorescence spectra

The UV-excited emission spectrum of DMANS in cyclohexane shows a feature at 425 nm (23 500 cm^{-1}) typical of fluorescence from a locally excited state. Raising the solvent polarity assists in reducing the emission energy, whereas raising the solvent viscosity plays a predominant role in increasing the emission intensity. While the solvent parameter Δf is a function of both the molecular polarity and refractivity [26], the Dirmoth parameter $E_T(30)$ is a function of the solvent polarity [27]. Figure 3 shows a linear dependence of the ICT emission energy on these solvent parameters. However, the emission intensity increases with the solvent viscosity reaching a maximum in glycerol. It appears that these solvent parameters reinforce one another for assisting the DMANS rigid ICT-stabilized structure $\mathbf{I}_y$, where emission in this case is more favoured to take place from the lower energy, more populated ICT state.

Low temperature measurements of DMANS emission in glycerol reveal a very interesting solvent dependence. Glycerol accommodates the ideal solvent conditions suitable for enhancing the fluorescence from the ICT state. Figure 4 shows the effect of reduced temperatures on the fluorescence

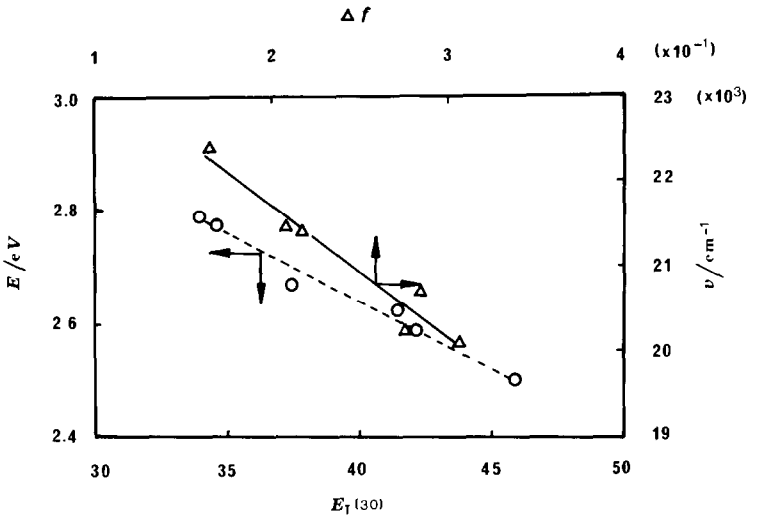

Fig. 3. Dependence of emission energy of DMANS ν and E, on the solvent parameters Δf and $E_T(30)$, respectively.

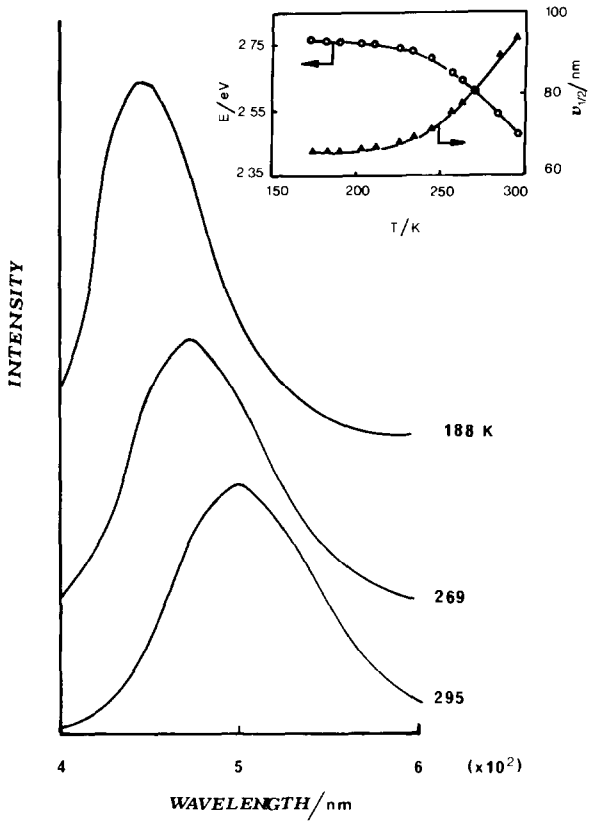

Fig. 4. Low temperature measurements of DMANS emission in glycerol. Inset shows the temperature dependence of the emission band width and energy.

of DMANS in glycerol. Three major aspects are observed upon progressively reducing the temperature, using a stream of liquid-nitrogen-cooled nitrogen gas (Fig. 4): (i) the half band width decreases, (ii) the peak height rises, and (iii) the peak maximum shifts to higher energies. Reducing the temperature appears to freeze the role of the solvent dipole so that it loses its feature of reducing the emission energy. However, the solvent viscosity is enhanced on cooling so that a faster emission with a higher quantum yield is favoured. All the changes demonstrate emission occurring from the locally excited state. This would explain the structural shift towards the more delocalized structure $\mathbf{I}_x$, which is less favoured at ordinary conditions. Figure 4 (inset) illustrates a very interesting dependence of the emission energy and half band width on temperature. The two dependencies equilibrate near 273 K. This might demonstrate the presence of a thermodynamic equilibrium. The $\mathbf{I}_x$ form is stabilized at low temperatures, whereas the $\mathbf{I}_y$ form is more favoured under ordinary conditions.

Based on these solid state and solution spectral data, it is concluded that DMANS is favourably located in the more rigid ICT structure $\mathbf{I}_y$ under ordinary conditions. Protonation retards the ICT phenomena and renders the molecule more delocalized as in structure $\mathbf{I}_x$. This allows a better accessibility to various molecular motions, which can be the origin of the phase transition induced in the protonated form in the solid state.

Thermal analysis

The interpretation of thermal features and shifts observed on protonation is facilitated by reference to structural information previously collated for this purpose.

The thermogram of DMANS (Fig. 5, curve **I**) shows a solid–liquid endothermic phase transition at 378 K. At higher temperatures, exothermic transitions are observed, which suggest decomposition via polycyclic products which are the precursors of coke formation. While protonation does not affect the decomposition, it influences significantly the molecular structure in two major aspects: (i) shift of the solid–liquid phase transition to a higher T_c of 438 K (Fig. 5, curve $\mathbf{II}_B$), and (ii) the appearance of a new solid state phase transition at lower T_c of 338 K (Fig. 5, curve $\mathbf{II}_A$). The former shift agrees with the transfer of the molecular structure from covalent to an ionic species, whereas the more important appearance of the solid state phase transition agrees with the transfer to the more flexible structure **II** (Scheme 1), where molecular rotation or twisting is more accessible. As the exothermic transitions are not shifted by protonation, discussion of the thermal data is limited to the shifts observed in the lower temperature range.

Figure 6 compares the C_p of both compounds. It is unambiguous to observe a great rise in the C_p of the solid–liquid (Fig. 6, curves I and $\mathbf{II}_B$)

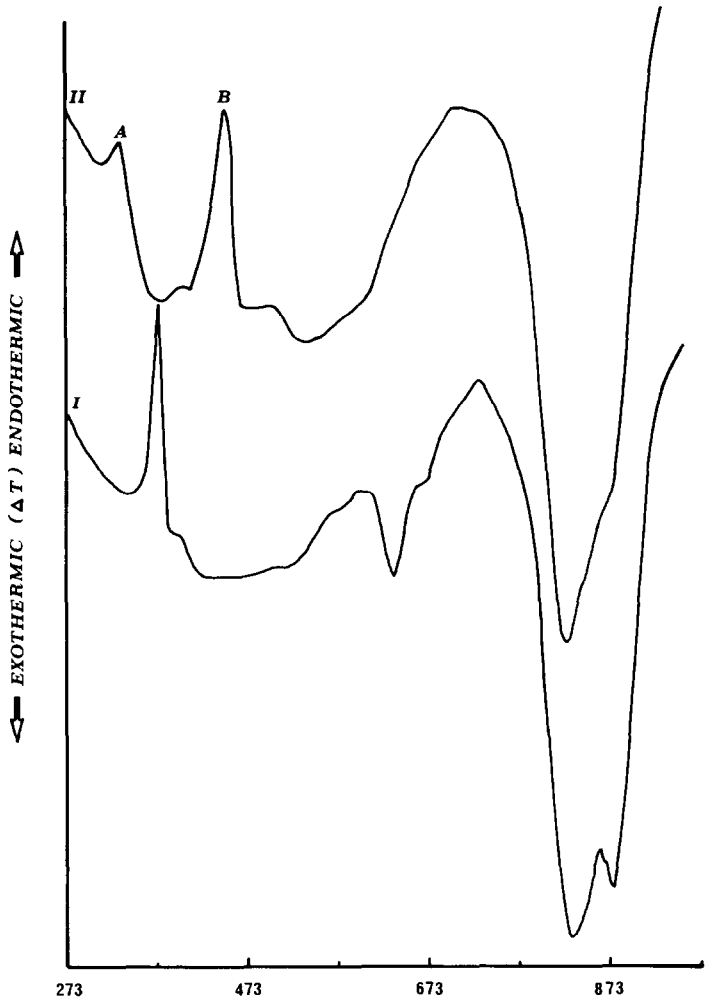

Fig. 5. DTA thermograms (273–973 K) of DMANS (I) and the protonated form (II) showing solid state (A) and solid–liquid (B) phase transitions.

phase transition, which should happen on the transfer to the protonated form of higher thermal stability. However, it is of particular interest to detect a newly induced endothermic solid state phase transition (Fig. 6, curve II_A) of lower C_p. The lower T_c and C_p of the latter transition would clarify the less energetic intramolecular rotation or twisting, as compared to the molecular translation resulting in the melting. Nevertheless, since the protonated form is of an ionic nature, the enthalpy changes ΔH (7.64 and 13.71 J g^{-1}) of its solid and melting phase transitions are higher than that (4.25 J g^{-1}) of the less thermally stable covalent DMANS. ΔH is calculated with reference to pure indium (28.4 J g^{-1}) observed at 703 K.

The activation energy of the transition is best calculated (far from the T_c [28]) from the slope of the linear dependence (Fig. 7 and eqn. (1)) of

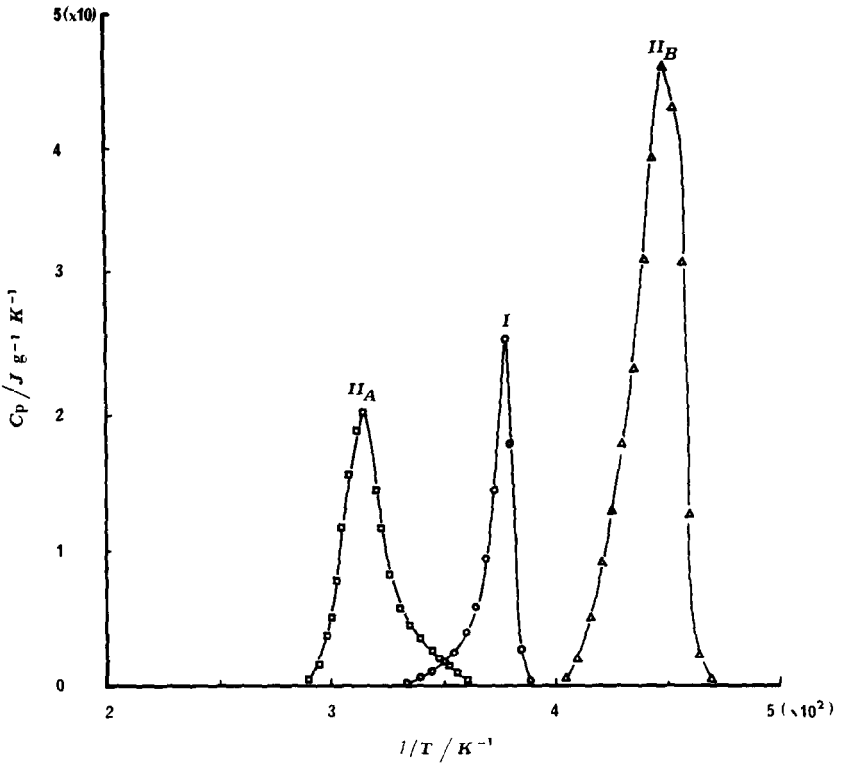

Fig. 6. Specific heats of DMANS solid–liquid phase transition (I) (○), and of the protonated form (II_A solid state (□) and II_B solid–liquid (△) phase transitions).

$\ln(C_pT^2)$ on T^{-1}

$$\ln(C_pT^2) = \ln(ZNU^2/R) - E^{\#}/RT \quad (1)$$

where Z is a coordination number, N the number of defects, R the universal gas constant and $E^{\#}$ the activation energy. Consistent with the enthalpy data and the stronger binding forces, the activation energies of the protonated form (155 and 295 kJ g^{-1} K^{-1}) solid and melting phase transitions, respectively, are higher than that (117 kJ g^{-1} K^{-1}) of the DMANS melting phase transition.

Finally, it is important to assign the model to which the phase transitions belong. This could be estimated (Fig. 8 and eqn. (2)) from the structural parameter α which is best calculated (near the T_c [29]) from the slope of the logarithmic linear dependence of

$$C_p = At^{-\alpha} \quad (2)$$

where A is a constant, $t = (T - T_c)/T_c$ and α is the thermodynamic parameter taken as a function of the transition model. It reveals a much

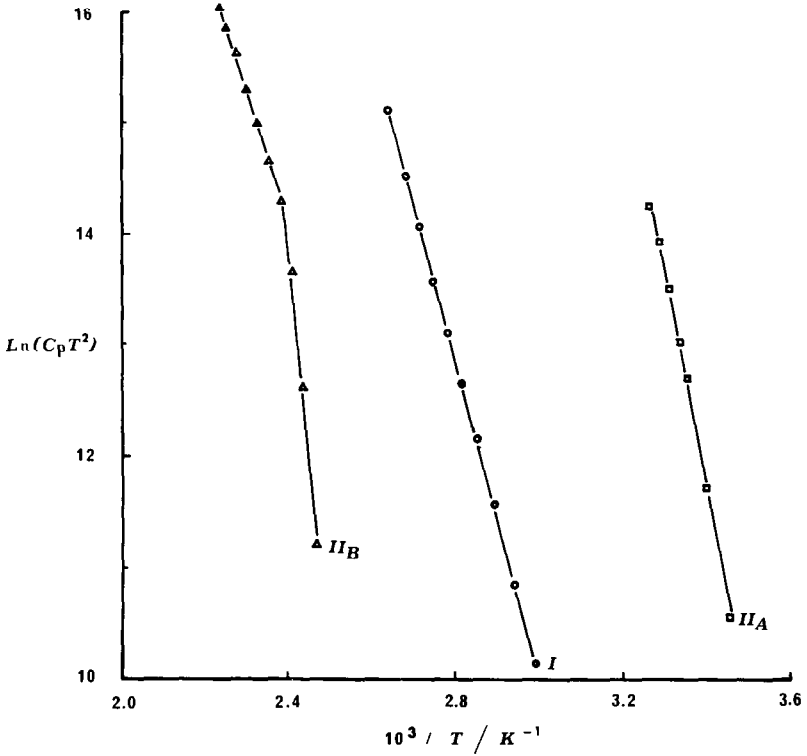

Fig. 7. Dependence of $\ln(C_pT^2)$ on T^{-1} for estimating the effect of protonation on the activation energy of DMANS phase transition. Symbol notation as in Fig. 6.

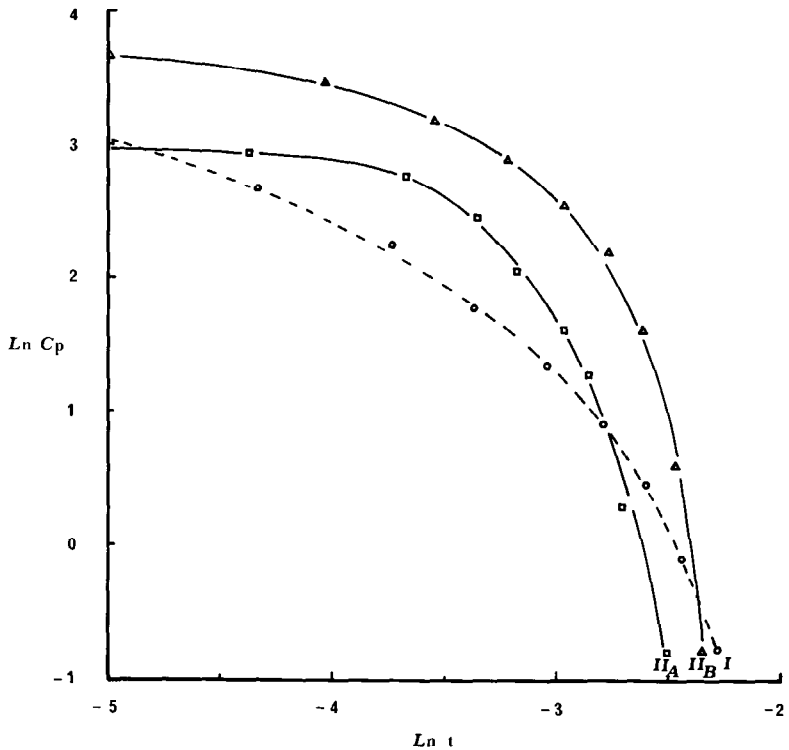

Fig. 8. Effect of protonation on the logarithmic dependence of C_p on the relative temperature change $(T - T_c)/T_c$ for estimating the proton-induced change in DMANS phase transition model. Symbol notation as in Fig. 6.

higher value of 0.64 for DMANS than those of 0.06 and 0.19 for the solid and melting phase transitions, respectively, of the protonated form. The high value of DMANS agrees with its highly ordered [30] and rigid ICT structure, whereas the much lower values of the protonated form are more compatible with the 3-d Ising model [31].

REFERENCES

1 M. Berthelot, Bull. Soc. Chim. Fr., 7 (1867) 30, 43.
2 E. Lippert, W. Lucler and H. Boos, in A. Manginin (Ed.), Advances in Molecular Spectroscopy, Pergamon, Oxford, 1962, p. 443.
3 W. Rettig and E. Lippert, J. Mol. Struct., 61 (1980) 17.
4 J. Boursou and B. Valeur, J. Phys. Chem., 93 (1984) 3871.
5 Z.R. Grabowski, J. Dobkowski and W. Kuhnle, J. Mol. Struct., 114 (1984) 93.
6 W. Rettig and A. Klock, Can. J. Chem., 63 (1985) 1649.
7 W. Rettig, Angew. Chem. Int. Ed. Engl., 25 (1986) 971.
8 A. Safarzadeh, Chem. Phys. Lett., 129 (1986) 225.
9 U. Leinhos, W. Kuhnle and K.A. Zachariasse, J. Phys. Chem., 95(5) (1991) 2013.
10 H. Gum and H. Garner, Z. Naturforsch., 389 (1983) 928.
11 J.M. Drake, M.L. Lesiecki and D.M. Camaioni, Chem. Phys. Lett., 113 (1985) 530.
12 A. Safarzadeh, Chem. Phys., 125 (1988) 145.
13 M. Vogel, W. Rettig, U. Fiedeldei and H. Baumgartel, Chem. Phys. Lett., 148 (1988) 347.
14 W. Rettig, M. Vogel and K.H. Drexhage, Chem. Phys. Lett., 147 (1988) 296, 452.
15 J. Jaraudias, J. Photochem., 13 (1980) 35.
16 R.H. Baker and M.J. Gratzel, J. Am. Chem. Soc., 102 (1980) 847.
17 R.O. Loutfy, Macromolecules, 14 (1981) 1970.
18 I.A. Al-Ansari, Photophysical studies on a series of *n*-(2,5-dimethoxyphenyl) arenes and *trans*-(*p*-*N*,*N*-dialkylaminobenzylidine)-1-naphthalenes, Ph.D. Dissertation, University of South California, 1991.
19 M.B. Sayed, M.E. Kassem and I.M. Al-Emadi, Thermochim. Acta, 188 (1991) 143.
20 H. Beens, H. Knibbe and A. Weller, J. Chem. Phys., 47 (1967) 1183.
21 G. Gones, W.R. Jackson and A.M. Halpern, Chem. Phys. Lett., 72 (1980) 391.
22 R. Tominaga and R.N. Castle, J. Heterocyclic Chem., 19 (1982) 1125.
23 J.M. Drake, M.L. Lesiecki and D.M. Camaioni, Chem. Phys. Lett., 92 (1985) 397.
24 L.J. Bellamy, The Infrared Spectra of Complex Molecules, Chapman and Hall, London, 1975.
25 I.B. Berlman (Ed.), Handbook of Fluorescence Spectra of Aromatic Molecules, Academic Press, New York, 1971.
26 E. Lippert, Z. Electrochem., 61 (1957) 962.
27 C. Riechardt, Angew. Chem., Int. Ed. Engl., 4 (1965) 29.
28 V.P. Burtseva, V. E. Vasilev and V.M. Varikash, Sov. Phys.-Solid State, 30(5) (1988) 877.
29 L.P. Kadanoff, W. Gotze, D. Hamblen, R. Hetch, E.A.S. Lewis, V.V. Palciauskas, M. Rayl, J. Swift, D. Aspnes and J. Kane, Rev. Mod. Phys., 29(2) (1967) 395.
30 G.H. Meissner and H. Hais, Acta Phys. Austriaca, Suppl., 18 (1977) 567.
31 D.S. Gaunt and C. Domb, J. Phys. C, 2(I) (1968) 1038.